Electrochimica Acta 348 (2020) 136345

Contents lists available at ScienceDirect

Electrochimica Acta

journal homepage: www.elsevier.com/locate/electacta

On neural network modeling to maximize the power output of PEMFCs

Fereshteh Salimi Nanadegani [a, b], Ebrahim Nemati Lay [a], Alfredo Iranzo [c], J. Antonio Salva [d], Bengt Sunden [b, *]

[a] Department of Chemical Engineering, University of Kashan, Ravand Street, Kashan, P.O. Box 87317-51167, Iran
[b] Department of Energy Sciences, Lund University, SE-22100, Lund, Sweden
[c] Thermal Engineering Group, Energy Engineering Department, School of Engineering, Universidad de Sevilla, Camino de Los Descubrimientos S/n, 41092, Sevilla, Spain
[d] AICIA, Camino de Los Descubrimientos S/n, 41092, Sevilla, Spain

ARTICLE INFO

Article history:
Received 1 January 2020
Received in revised form
16 March 2020
Accepted 28 April 2020
Available online 29 April 2020

Keywords:
PEMFC
Artificial neural network
Operation optimization
Polarization curve
Water management

ABSTRACT

Optimum operating conditions of a fuel cell will provide its maximum efficiency and the operating cost will be minimized. Thus, operation optimization of the fuel cell is essential. Neural networks can simulate systems without using simplifying assumptions. Therefore, the neural network can be used to simulate complex systems. This paper investigates the effects of important parameters, i.e., temperature, relative humidity in the cathode and anode, stoichiometry on the cathode and anode sides, on the polarization curve of a PEMFC (Proton Exchange Membrane Fuel Cell) having MPL (Micro Porous Layer) by ANN (artificial neural network). For this purpose, an analytical model validated using laboratory data is applied for prediction of the operating conditions providing maximum (and/or minimum) output power of a PEM fuel cell for arbitrary values of the current. The mean absolute relative error was calculated to 1.95%, indicating that the network results represented the laboratory data very accurately. The results show 23.6% and 28.9% increase of the power by the model and the network, respectively, when comparing the maximum and minimum power outputs.

1. Introduction

Fuel cells (FCs) can provide efficient energy conversion with a low impact on the environment and accordingly they are considered as a potential source of alternative energy. FCs are of interest in the production of independent commercial electricity, residential applications, and power plants. PEMFCs usually operate at low temperatures and may provide benefits like high energy density as well as safe operation etc. Due to the low operating temperature and good performance, PEMFCs are nowadays of great interest in providing power for the propulsion in the automotive field [1].

Nevertheless, there are several barriers that have to be overcome, e.g., high cost, weight, and volume, to make PEMFCs competitive to traditional engine power systems, i.e., internal combustion engines [2–4]. Mathematical models and simulations are then needed to enable design and performance improvements and to optimize the operating conditions so that the output and efficiency of the fuel cell can be increased [5]. The operating conditions play a significant role in the PEMFC performance [6,7]. The performance optimization is a key approach to achieve a cost reduction in PEMFCs, as more compact stacks can be achieved featuring a reduced number of cells for a given power output.

The method of artificial neural network (ANN) is known to be a powerful tool in nonlinear modeling [8]. Several different ANN models to optimize PEMFC operations [8–14] have been presented and these include static and dynamic states, see Table 1.

A model for the management of water was developed by Zhang et al. [15]. Using a repeated neural network optimization (RNN), a prediction model control mechanism was proposed. The models were implemented in MATLAB and SIMULINK environments. The simulations revealed that by using this method, fluctuations in water concentration in the cathode could be avoided and accordingly the lifetime of the PEMFC stack could be prolonged. In another study, Lebreton et al. [16] approved a Fault Tolerance Control

* Corresponding author.
E-mail addresses: fereshtehsalimi@alumni.ut.ac.ir (F.S. Nanadegani), enemati@kashanu.ac.ir (E.N. Lay), airanzo@us.es (A. Iranzo), Jose.Salva@kelvion.com (J.A. Salva), bengt.sunden@energy.lth.se (B. Sunden).

https://doi.org/10.1016/j.electacta.2020.136345
0013-4686/

Table 1
Applications of ANN for PEMFCs modeling.

References	Input variables	Output variables
Jemei et al. [8] (2003)	Current and temperature in the stack, flow rates of hydrogen and oxygen	Optimization of voltage
Jemei et al. [9] (2008)	Flow and temperature in the stack, flow rates of oxygen and hydrogen, air humidity	Optimization of voltage
Sisworahardjo et al. [10] (2010)	Current and temperature in the stack	Voltage, power, hydrogen flow rate
Yousfi-Steiner [11] (2011)	Current and temperature in the stack, flow rates, dew point temperature	Voltage, pressure drop
Chang [1] (2011)	Operating temperature, flow rates of hydrogen and oxygen, current load, pressure on oxygen and hydrogen sides	Optimization of Output, Voltage
Damour et al. [12] (2013)	Flow rates of air and hydrogen, Operating temperature	Power
Curteanu et al. [13] (2014)	Current density, C/PBI, mean pore size, tortuosity, porosity	Optimization of fuel cell efficiency
Han et al. [14] (2016)	Cooling water temperature, air temperature, temperature difference of cooling water, flow, air flow rate	Optimization of system efficiency

Strategy (FTCS) for PEMFC water management and validated it for a real PEMFC system. A combined method of the sequential neural-network approximation and orthogonal arrays (SNAOA) to determine the performance parameters in the operation of PEMFCs was presented by Chang [17].

A number of articles have used other methods to optimize the operation of a single PEMFC [5,18–23]. Salva et al. [5] conducted an optimization study to maximize the performance polarization curve with EES (solving the engineering equation). Mawardi et al. [18] suggested an optimization model maximize the power density of a PEMFC. The numerical model of the fuel cells was solved using simulated annealing and a simplex search algorithm. The Taguchi method was applied by Kaytakoglu and Akyalcin [19] to find the optimal operating conditions for maximum PEMFC power density. Askarzadeh and Rezazadeh [20] applied a modified particle swarm optimization (MPSO) method for a PEMFC. They proved that the MPSO can be regarded as a useful and reliable method to optimize the model parameters. They claimed that also it might be applicable for solving other complex problems of optimization of fuel cells. Meidanshahi and Karimi [21] considered a nonlinear dynamic model for a PEMFC analysis in one dimension. The operating conditions of the cell were optimized at steady-state conditions in order to obtain the most suitable parameters for achieving the highest and most uniform distribution of the current density. The differential evolution (DE) was used as an optimization algorithm. Zhang et al. [22] determined the optimum temperature of a high-temperature PEMFC in terms of performance and CO tolerance as well as durability. Kanani et al. [23] applied the response surface method (RSM) to find out the maximum power of a single PEMFC.

In addition, in other works ([24,25]) parameter optimization of a PEMFC stack has been investigated. A niche hybrid genetic algorithm (HGA) was used by Mo et al. [24] to optimize a PEMFC. The input-output data used by them were output-voltage and demand current of the stack, cathode and anode pressures. Their genetic algorithm is a modified one and they found that it might be effective and reliable to optimize the model parameters of a PEMFC. Liu et al. [25] used an orthogonal experimental design for the optimization of the performance of a PEMFC stack. For this purpose, the operating parameters included operating temperature, stoichiometry in the cathode, relative humidity as well as back-pressure. The results revealed that operating temperature and stoichiometry in the cathode side have a greater impact on the output voltage and efficiency of the stack compared to other parameters.

The ANN has advantages over other analytical methods. Among these, it is worthwhile to mention the use of fewer assumptions for modeling and excellent non-linear approximation ability. In addition, an incomplete database can be applied and it has a low sensitivity to noise [26].

In this paper, the artificial neural network is applied to find the operating conditions which maximize and/or minimize the power output. An analytical one-dimensional model introduced by Salva et al. [27] is used as a dataset for the ANN network (section 2). This model simulates the main phenomena occurring during the fuel cell operation, i.e., electrochemistry, mass transport (gas and liquid) and heat transfer. In addition, the analytical model has been thoroughly validated versus experimental data including cell voltage and water content inside the PEMFC (Tests were conducted in the previous work [5] for a 50 cm^2 fuel cell). Two parameters were used simultaneously in the validation process to ensure that the results are accurate. Validation was carried out for different operating conditions, i.e., temperature, cathode and anode stoichiometry, and relative humidity in the cathode and anode. The NeuroSolutions software [28] is used to simulate and analyze a PEMFC performance using an artificial neural network (ANN) approach. There are three basic steps in developing the neural network, namely network training on the data, network testing for accuracy, and creating predictions/classifications from new data. The NeuroSolutions Excel can handle this entirely automatically in one simple step [28]. The main novelty of the current work is the analysis of a PEMFC with an MPL and maximizing the operating conditions for any current. The ANN model can simulate the system without using simplifying assumptions and to provide a powerful optimization tool.

2. The single PEMFC performance

The single cell voltage (V_{cell}) is given by Eq. (1), [6,7].

$$V_{cell} = E^0(T,P) - \eta_{a,a} - |\eta_{a,c}| - \eta_r - \eta_{m,a} - |\eta_{m,c}| \quad (1)$$

where $E^0(T,P)$represents the equilibrium open-circuit potential of the cell (V), $\eta_{a,c}$and $\eta_{a,a}$are the activation overpotentials in the cathode and anode (V), respectively, η_r is the ohmic overpotential (V) while and $\eta_{m,a}$are the concentration overpotentials in the cathode and anode (V), respectively.

2.1. Equilibrium open-circuit potential

From Nernst equation, one finds the equilibrium open-circuit potential as given by equation. (2), [29,30].

$$E^0(T,P) = \frac{-^\circ G^0(T)}{nF} + \frac{RT}{nF} ln \left(\frac{\left(\frac{y_{H_2} P_{anode}}{P^0}\right)\left(\frac{y_{O_2} P_{cathode}}{P^0}\right)^{\frac{1}{2}}}{\left(\frac{y_{H_2O} P_{cathode}}{P_{sat}(T)}\right)} \right) \quad (2)$$

where $^\circ G^0(T)$, R, F, P^0, P_{sat}, $P_{anode/cathode}$ are the Gibbs free energy (J), ideal gas constant (8.314 J/moleK), Faraday constant (96,487C/mole), reference pressure (Pa), saturation pressure (Pa), operating pressure in anode and cathode (Pa), respectively, n is the number of moles of electrons in a reaction (2 for anode side and 4 for cathode side), y_i represents hydrogen mole fraction at the anode and water and oxygen mole fraction, respectively, at the cathode.

2.2. Calculation of activation overpotentials

The activation overpotentials are calculated by using the Tafel simplification [6,7] and are given by Eqs. (3) and (4).

$$\eta_{a,a} = \frac{RT}{\alpha_a F} ln\left(\frac{i}{i_{0,a}}\right) \quad (3)$$

$$\eta_{a,c} = \frac{RT}{\alpha_c F} ln\left(\frac{i}{i_{0,c}}\right) \quad (4)$$

where T and i represent operating temperature (^{o}C) and current density (A/m^2), respectively, α_c and α_a are the charge transfer coefficients at the cathode and anode, respectively, while $i_{0,c}$ and $i_{0,a}$ are exchange current densities in the cathode and anode (A/m^2), respectively.

Eqs. (5) and (6) are used to calculate the exchange current densities, [6].

$$i_{0,a} = i_{ref,a}\left(\frac{C_{a,GDL-CL}}{C_{ref}}\right)^{\gamma_a} exp\left(-\frac{E_{a,a}}{RT}\right) \quad (5)$$

$$i_{0,c} = i_{ref,c}\left(\frac{C_{c,GDL-CL}}{C_{ref}}\right)^{\gamma_c} exp\left(-\frac{E_{a,c}}{RT}\right) \quad (6)$$

where $i_{ref,a}$ and $i_{ref,c}$ are the reference values of the exchange current densities without concentration losses and at a certain reference temperature for the anode or cathode (A/m^2), respectively. $C_{c,GDL-CL}$ and $C_{a,GDL-CL}$ represent the oxygen or hydrogen concentration at the cathode and anode side (mol/m^3), respectively. The activation energies, $E_{a,a}$ and $E_{a,c}$, are valid at the anode and cathode electrodes (J/mol), respectively. C_{ref} is a reference concentration (mol/m^3), and γ_i means the reaction order of the elementary charge transfer step.

2.3. Calculation of the ohmic overpotential

The electrical conductivity and thickness of the bipolar plates, GDLs, CLs, MPLs and the membrane affect the ohmic overpotential. In addition, as the contact resistance at the interface between the GDL and bipolar plate affects the performance of the fuel cell, it is included in the ohmic overpotential [31].

The ohmic overpotential is calculated by Eq. (7) [32].

$$\eta_r = i\left(2\frac{t_{BP}}{\sigma_{BP}} + 2\frac{t_{GDL}}{\sigma_{GDL}} + 2\frac{t_{MPL}}{\sigma_{MPL}} + 2\frac{t_{CL}}{\sigma_{CL}} + \frac{t_{Mem}}{\sigma_{Mem}} + 2R_{contact}\right) \quad (7)$$

where t_i and σ_i are thickness (m) and electrical conductivity (1/Ωm), respectively, of the BP (bipolar plate), GDLs, MPLs, CLs and the MEA (membrane electrode assembly). $R_{contact}$ is the contact resistance at the interface between the GDL and bipolar plate (Ωm^2).

The electrical conductivities were picked up in available datasheets for each material [33–35]. The membrane protonic conductivity is a function of the water content and is calculated by Eq. (8) [36].

$$\sigma_{membrane} = exp\left(1268\left(\frac{1}{303} - \frac{1}{T}\right)\right)(0.005193\lambda - 0.00326) \quad (8)$$

where λ denotes the water content inside the membrane. This parameter is calculated by Eq. (9) [6,31,32,37].

$$\lambda = \begin{cases} ^\circ 0.043 + 17.18a - 39.85a^2 + 36a^2 & if\ a < 1 \\ ^\circ 14 + 14(a-1) & if\ a > 1 \end{cases} \quad (9)$$

where a is the water activity which is calculated by Eqs. (10)-(12), [31,37].

$$a_a = \frac{C^{mem}_{H_2O,a} RT}{P_{sat}} \quad (10)$$

$$a_c = \frac{C^{mem}_{H_2O,c} RT}{P_{sat}} \quad (11)$$

$$a = \frac{a_a + a_c}{2} \quad (12)$$

where $C^{mem}_{H_2O,a}$ and $C^{mem}_{H_2O,c}$, respectively, represent the water concentrations at the anode and cathode sides (mol/m^3) of the membrane.

2.4. Calculation of the concentration overpotentials

The expressions to calculate the concentration overpotentials are shown in Eqs. (13) and (14), [6,7].

$$\eta_{m,a} = -\frac{RT}{n_a F} * ln\left(1 - \frac{i}{i_{lim,a}}\right) \quad (13)$$

$$\eta_{m,c} = -\frac{RT}{n_c F} * ln\left(1 - \frac{i}{i_{lim,c}}\right) \quad (14)$$

where n_i is the number moles of electrons in the reactions (2 for anode side and 4 for cathode side) and $i_{lim,i}$ is the limiting current density at the cathode or anode sides. The limiting current densities can be found, e.g., experimentally.

3. Artificial neural network (ANN)

An artificial neural network (ANN) is built up of a number of elementary processing units, called neurons, which are connected together into a neural network. The relationship between two neurons is handled by weight functions [11].

With an available set of input and output data, the ANN is able to learn and construct non-linear mappings providing incentive solutions for modeling complex systems, especially those that are known to be without variable relationships. Concerning the structure of neural networks, two basic topologies exist, namely feed-

forward networks and recurrent networks. In the feed-forward network, outputs of a certain layer are inputs of the following adjacent layer. The so-called hidden layers are situated between the input nodes and the output layer [38].

Among the different ANNs, the MLP (Multi-Layer Perceptron) type is the most common one used in PEMFC modeling [39]. The MLP has three sections: the input layer, the output layer, and the intermediate or hidden layer. Any section can have several layers. Each unit performs a biased weighted sum of the inputs and sends this information to a transfer function. The output is given by the activation level of this transfer function. The organization of neurons is a set of parallel layers [11].

When the numbers of layers and neurons within these layers are fixed, training algorithms are applied to determine the network weights. The main purpose is to minimize the deviation between the calculated output from the neural network and an experiment. There are many techniques for training a neural network. The two main techniques employed by neural networks are known as supervised learning and unsupervised learning. The most common supervised training algorithm is known as back-propagation [39]. Network training with back-propagation algorithms requires the steps described below:

- A set of examples is assembled for the network training. Each item includes inputs into the network and the corresponding solution which represents the desired output from the network.
- The network output is calculated.
- The deviation between the output of the network and the target vector of the learning pair is calculated.
- The network weights are set in a way that minimizes the error.
- Steps 1–4 are repeated for each vector in the instruction class to reduce the error for the entire class in a way that is acceptable.

By providing each set of information to the network, weights are corrected. Once the entire data set has been given to the network, an epoch has been completed. Another issue addressed in the learning algorithm is when the training should end. To do this, one of the following three methods can be used:

- A constant value for the number of times (epoch) is to provide the total data to the network. If the results are not satisfactory at the end of the training, the steps will be repeated again.
- During the training, after every round of data provided to the network, training is temporarily stopped and the network performance is measured. Network performance measurement can be conducted against a training series or a Cross-Validation Data series.
- The two above methods as graduation criteria can be combined.

Generally, the performance of a neural network is tested against a cross-validation data series to judge the future outcome of the network and prevent over-network training.

A suitable learning algorithm for training MLPs is the Genetic Algorithm (GA). GA imitates natural evolution. A population of chromosomes is a better solution due to different selection, crossover, and mutation. A uniform distribution of the population is randomly assigned primarily and the number of chromosomes contained is described by the population size. The chromosomes include optimized parameters and evaluation of the value of the solution is done using a fit function. This method is repeated many times and a parameter named “number of generations” is defined [40]. Genetic algorithms are generally applied in four procedures [28]:

- Best inputs to the neural network are chosen;
- Neural network parameters are optimized;
- Training of actual network weights;
- Choose/modify neural network architecture.

In this study, the procedure to design the networks was implemented by the NeuroSolutions software [28]. Users can train a neural network and test its performance directly in this software. In addition, this software has powerful built-in features which can be used to genetically optimize the network parameters. The software combines a neural network and a genetic algorithm to obtain the optimal network size and parameters [41].

4. Application of NeuroSolutions for excel

The NeuroSolutions software is used as it has powerful built-in features that can find the optimal neural network for a problem. These are genetically optimization of the network parameters, ability to train a neural network multiple times, and changing each neural network parameter in several implementations. NeuroSolutions for Excel is broken down into five major modules that are used to create and train a network. These modules are shown in Fig. 1 [42] and described below.

4.1. Preprocess data

This module is used to apply different preprocessing techniques to the raw data to provide it as input into the neural network.

4.2. Tag data

This module is used to graphically tag portions of the data as Training Input, Training Desired, Cross-Validation Input, Cross-Validation Desired, Testing Input, and Testing Desired.

- Column(s) as Input: The selection of this menu item allows one to tag columns of data as Input.
- Column(s) as Desired: The selection of this menu item allows one to tag columns of data as Desired.
- Rows by percentages: The selection of this menu item provides a quick method for tagging multiple rows of data. Selection of this sub-menu item allows one to enter the percentages (of the total number of rows) to tag as Cross-Validation and Testing. The remaining part of the data will be tagged as Training.

4.3. Create/open network

This module is used to create a NeuroSolutions breadboard (neural network).

4.4. Training the network

This module is used to train a network using one of the several built-in training processes. This powerful module permits the user to easily find the optimum network for a particular problem.

- Train Genetic: The selection of this option trains the active NeuroSolutions breadboard while genetically optimizing the network choice of inputs, step sizes, momentum values, and the number of processing elements in the hidden layer(s). Other parameters can also be optimized by setting them up manually within NeuroSolutions. The goal of the optimization is to find the parameter settings that result in a minimum error. If cross-validation is used, the goal will be to minimize the cross-validation error. Otherwise, the goal will be to minimize the

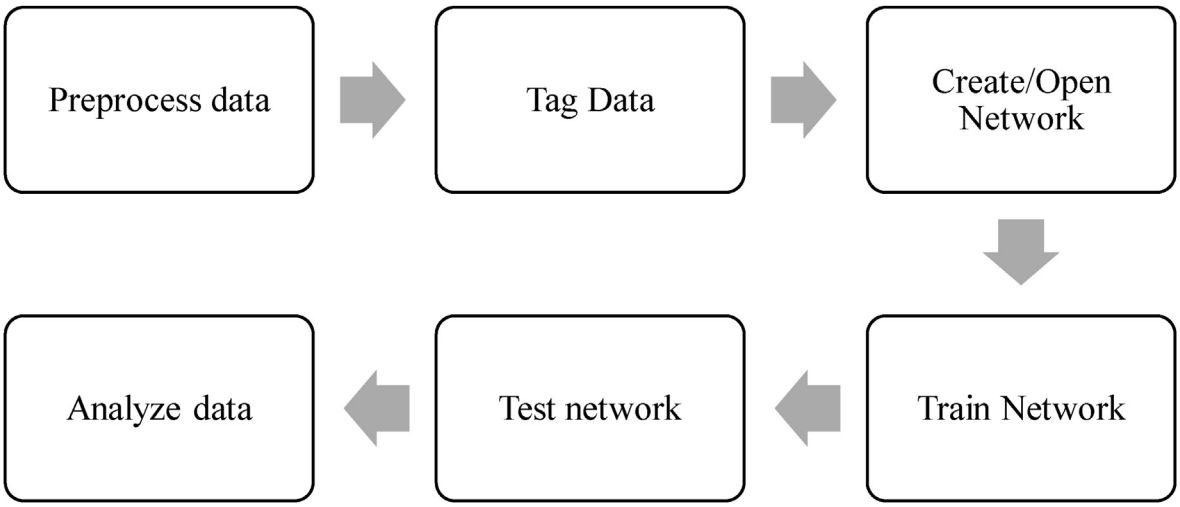

Fig. 1. Flow diagram for methodology of work with NeuroSolutions software.

training error. To perform genetic training, first, an initial population of networks is randomly created, each having a different set of parameters. Each of these networks is then trained and evaluated (to determine its fitness) based on the minimum error achieved. The characteristics of the good networks are then combined and mutated to create a new population of networks. Again, the networks in this population are evaluated and the characteristics of the best networks are passed along to the next generation of networks. This process is repeated until the maximum generations or maximum evolution time is reached or the user stops the evolution.

- Train: The selection of this menu item, the active NeuroSolutions breadboard is trained one time and the best network weights are saved.

4.5. Tests of the network

This module is used to test the network after the optimum network has been found using the Train Network module. In testing the network, various performance measures are computed.

4.6. Analyze the network

This model aims to analyze the findings.

5. On designing the fuel cell artificial neural network

In this study, the process of designing the network is implemented by NeuroSolutions, where the MLP model of the neural network is constructed. The topology of the network is depicted in Fig. 2. As can be seen in this Figure, the network includes one input layer, two hidden layers, and one output layer. Network inputs are operation temperature, relative humidity, anode stoichiometry, cathode stoichiometry as well as current. The output of the network is the voltage. Table 2 shows the ranges of network input parameters. The hyperbolic tangent activation function ($f(x) = \tanh(x) = \frac{e^x - e^{-x}}{e^x + e^{-x}}$) is used for the hidden and output layers.

To create the network, 1296 series of data, 1296 inputs (T, i, RH, anode stoichiometry and cathode stoichiometry) were used. For

Table 2
Ranges of network input parameters.

Parameter	Range
Current (A)	0–15
λ_a	1.5, 3, 5
λ_c	2, 3, 5
$RH_{c/a}$ (%)	50, 80, 100
T (C^o)	50, 60, 70

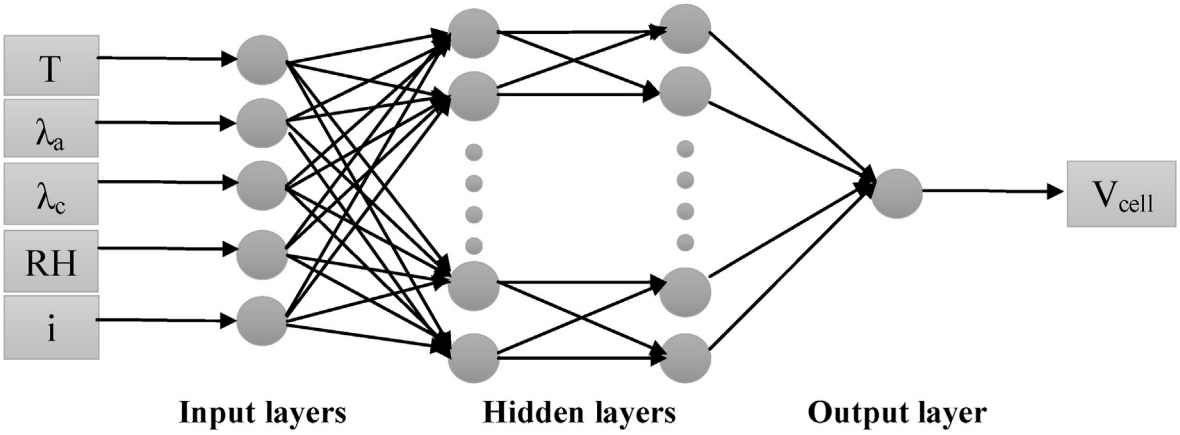

Fig. 2. Illustration of a feed-forward neural network.

each of these, there is one input, and accordingly we have 1296 outputs. The data were randomly divided into three independent subsets, namely 70% for training, 20% for cross-validation and 10% for tests. This division ensures that each subset contains the same amount of data from any operating mode as the initial dataset [11].

The number of neurons in the first and the second hidden layers of the network was 40 and 45, respectively. It should be noted that there is no precise method allowing the selection of the optimal neuron number in the hidden layers. In this work, a "trial-and-error" procedure is adopted. It starts from a small number of neurons and this number is successively increased until an acceptable compromise between complexity and performance of the model is achieved [11]. Associated with this procedure, the mean square error of the difference between the response values of the experimental data and the model data was calculated. The Levenberg–Marquardt procedure is selected for the learning rule and the number of the maximum epoch was set to 1000.

The training algorithm used was GA (Train Genetic option as indicated in Section 4.4), which performs the training while genetically optimizing the network's choice of inputs, step sizes, momentum values, and the number of processing elements in the hidden layers. The goal of the optimization is to find the parameter settings that result in the minimum error (minimize the training error). The software creates first a random initial population of networks with each a different set of parameters. Each of these networks is then trained and evaluated to determine its fitness based on the minimum error achieved. The characteristics of the good networks are then combined and mutated to create a new population of networks. After a new evaluation, the characteristics of the best networks are passed along to the next generation of networks. The parameters of GA that were chosen were: Number of Epoch: 1000; Population size: 50; Maximum generations: 100; Maximum evaluation time: 60.

Table 3 reports the performance of networks 1 to 4 in terms of the mean square error (MSE), the root mean square error (RMSE), and the linear correlation coefficient (r) between model data and neural network outputs. The MSE and RMSE are defined in Eqs. (15) and (16) below.

$$\mathrm{MSE} = \frac{1}{N}\sum_{i=1}^{N}(\text{desired output} - \text{network output})^2 \tag{15}$$

$$\mathrm{RMSE} = \sqrt{\frac{1}{N}\sum_{i=1}^{N}(\text{desired output} - \text{network output})^2} \tag{16}$$

6. Results and discussion

6.1. Experimental validation

To find the fuel cell polarization curve, three experiments were performed. These were conducted in previous work [5] for a 50 cm^2 fuel cell. The operating conditions for these three experiments are provided in Table 4. The validation of the model [27] is presented in Fig. 3. The polarization curves obtained by the model correspond well with the experimental data. Average absolute relative errors (AARE) are used to compare the experimental data with the results from the model and are calculated by Eq. (17).

$$\mathrm{AARE} = \frac{1}{N}\sum_{i=1}^{N}\left|\frac{\text{Model value} - \text{Experimental value}}{\text{Experimental value}}\right| \tag{17}$$

The results show that Test 1, Test 2 and Test 3 achieved 3.68%, 2.80% and 2.01% of the AARE, respectively, indicating that good matching between the model and experimental data has been reached.

Table 4
Operating conditions in the three tests.

	T (C°)	P (bar)	$RH_{c/a}$ (%)	λ_a	λ_c
Test 1	50	1	50	1.5	2
Test 2	50	1	100	1.5	2
Test 3	50	1	100	1.5	3.5

6.2. Optimization results

The output results of the neural network trained by the genetic algorithm in comparison with the model results suggested by Salva et al. [27] are presented in Fig. 4. According to this Fig. and 1.95% of AARE, the network training is deemed successful by the genetic algorithm and good agreement between network results and model results is found.

According to the results obtained from the neural network, the operating conditions offering maximum power output and the cell voltage corresponding to these conditions are shown in Table 5. The polarization curve with the best performance appears due to a combination of four different polarization curves.

- Set 1: T = 70 °C, $RH_{a/c}$ = 100%, $\lambda_a = 5$, $\lambda_c = 5$
- Set 2: T = 70 °C, $RH_{a/c}$ = 100%, $\lambda_a = 5$, $\lambda_c = 2$
- Set 3: T = 60 °C, $RH_{a/c}$ = 100%, $\lambda_a = 5$, $\lambda_c = 2$
- Set 4: T = 60 °C, $RH_{a/c}$ = 80%, $\lambda_a = 3$, $\lambda_c = 3$

Differences between the different sets confirm the importance of choosing appropriate operating conditions for various currents. The polarization curves, as well as the maximum performance of the PEMFC for the four different operating conditions, are shown in Fig. 5.

It is observed that for low currents, the optimal operating conditions appear at high temperatures, high relative humidity, high stoichiometry at the cathode and anode sides. If the current is increased, the outputs of the network recommend a reduction of the temperature from 70 °C to 60 °C. In addition, cathode stoichiometry should be reduced from 5 to 2, but anode stoichiometry is at the maximum value. This is because an increase in the temperature also increases the limiting current density [43]. Hydrogen is

Table 3
Performance of GA-ANN model.

Performance		Run 1	Run 2	Run 3	Run 4
Number of neurons	First layer	10	15	35	40
	Second layer	10	15	40	45
MSE		0.09851	0.01546	0.00276	0.00038
RMSE		0.31386	0.12433	0.05254	0.01949
r		0.9591	0.9635	0.9761	0.9876

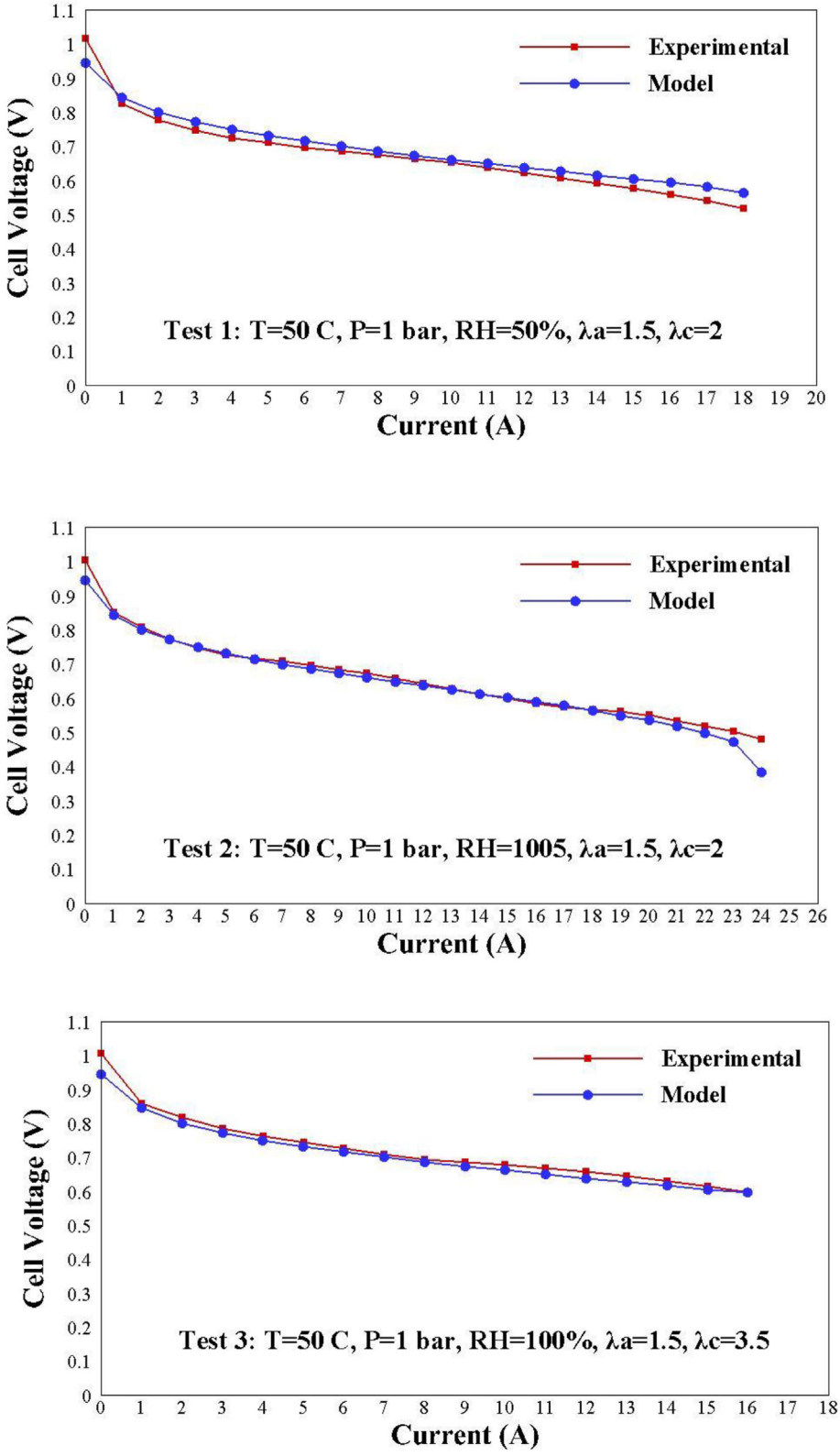

Fig. 3. Validation of the model versus experiments in terms of polarization curves.

transferred from the flow channels at a much faster rate at high currents, but within the air cathode, excessive water is produced in the form of liquid. This creates a gas-liquid two-phase flow in the porous cathode electrode. Transport of two-phase gaseous reactants to the reaction surface, i.e., the cathode-membrane interface, then becomes a mass transfer limiting mechanism [44]. In Fig. 5, the set 4 shows an abnormal behavior at a current around 13 A. A similar thing is also reflected in Fig. 6. This might be due the

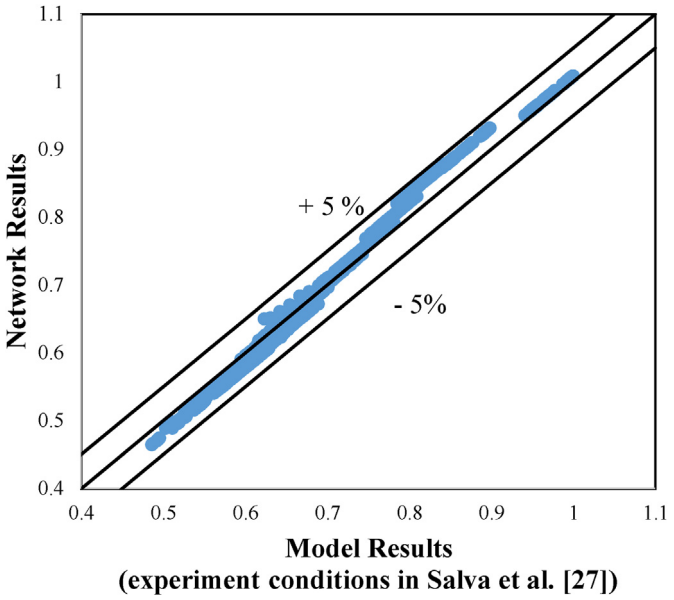

Fig. 4. Comparison of optimization results (network results) with model results of Salva et al. [27].

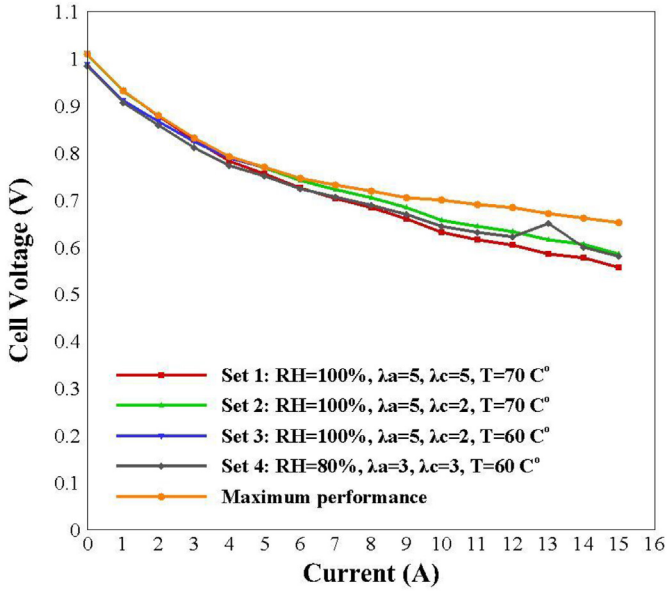

Fig. 5. Polarization curves for four different operating conditions and maximum performance.

Table 5
Operating conditions for the maximum power.

Current (A)	λ_a	λ_c	$RH_{c/a}$ (%)	T (C°)	Cell voltage (V)
0	5	5	100	70	1.0090
1	5	5	100	70	0.9321
2	5	2	100	70	0.8795
3	5	2	100	70	0.8315
4	5	2	100	70	0.7920
5	5	2	100	60	0.7700
6	5	2	100	60	0.7463
7	5	2	100	60	0.7309
8	5	2	100	60	0.7184
9	5	2	100	60	0.7043
10	5	2	100	60	0.7002
11	5	2	100	60	0.6902
12	5	2	100	60	0.6840
13	3	3	80	60	0.6710
14	5	2	100	60	0.6612
15	5	2	100	60	0.6523

fact that the relative humidity has its minimum value at this current.

At a certain limited range of the operating parameters, besides the operating conditions offering maximum power output and corresponding cell voltages, there are some operating conditions offering minimum power and corresponding cell voltages. Those conditions are shown in Table 6 for various currents (based on network results). These results clearly show that selecting operating conditions is important to increase the output power of a specific PEM fuel cell [5]. The polarization curve with the worst performance is found by combining three different polarization curves.

- Set 5: T = 50 °C, $RH_{a/c}$ = 50%, λ_a = 1.5, λ_c = 5
- Set 6: T = 60 °C, $RH_{a/c}$ = 50%, λ_a = 1.5, λ_c = 5
- Set 7: T = 50 °C, $RH_{a/c}$ = 100%, λ_a = 5, λ_c = 2

The polarization curves corresponding to these three operating conditions and the minimum performance of the PEMFC are shown in Fig. 6. It is observed that at low currents, high stoichiometry at

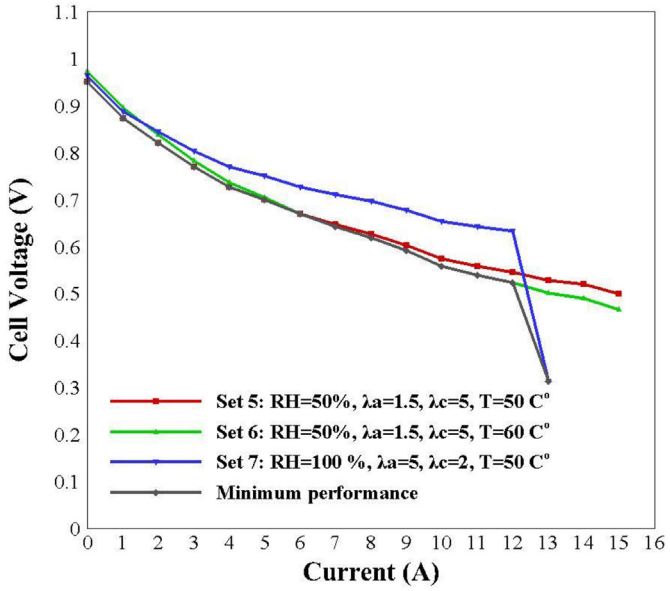

Fig. 6. Polarization curves for three operating conditions and the minimum performance.

the cathode, low temperature, and relative humidity, as well as low stoichiometry at the anode provide the lowest power and worst performance. On the other hand, under these conditions, the activation losses are the highest [5]. By increasing the current, the network results show only a change with temperature and the PEMFC performance will change. An increase of the temperature from 50 °C to 60 °C increases the ohmic losses and dry-out of the membrane takes place [5].

At a current of 13 A, the cell shows the lowest power. The operating condition at this current shows the maximum value of relative humidity. This result is according to the literature because humidification is not important at high currents. The reason is that dehydration may occur at the anode side and flooding at the

Table 6
Operating conditions for minimum power.

Current (A)	λ_a	λ_c	$RH_{c/a}$ (%)	T (C°)	Cell voltage (V)
0	1.5	5	50	50	0.9502
1	1.5	5	50	50	0.8733
2	1.5	5	50	50	0.8261
3	1.5	5	50	50	0.7693
4	1.5	5	50	50	0.7266
5	1.5	5	50	50	0.9698
6	1.5	5	50	50	0.6688
7	1.5	5	50	60	0.6426
8	1.5	5	50	60	0.6185
9	1.5	5	50	60	0.5906
10	1.5	5	50	60	0.5581
11	1.5	5	50	60	0.5389
12	1.5	5	50	60	0.5229
13	5	2	100	50	0.3131

cathode side. Accordingly, the humidifying of the cathode gas stream is not meaningful [45].

The polarization curve and the power curve for maximum and minimum performance are presented in Fig. 7. This figure confirms the very good agreement between the network and the model. The network results of the output power indicate that for the operating conditions of maximum performance, the power value reaches 9.78 W at 15 A. On the other hand, the maximum output power with minimum operating conditions is about 4.07 W at 13 A. A comparison between the operating condition of maximum performance with the operating condition of minimum performance, at a reference current of 12 A, shows 23.6% (8.02 W versus 6.49 W) and 28.9% (8.16 W versus 6.33 W) increase of the power by the model and the network, respectively.

6.3. Optimization of the operating conditions

In the following, the network results are used to predict the influence on the PEMFC performance based on changes in the operating conditions. As high temperature, high relative humidity, high stoichiometry at the cathode and anode sides provide the best performance (see section 4.2), these conditions (T = 70 °C, $RH_{a/c}$ = 100%, $\lambda_a = 5$, $\lambda_c = 5$) are selected as the fixed condition.

Fig. 8 depicts the effect of the operating temperature of the

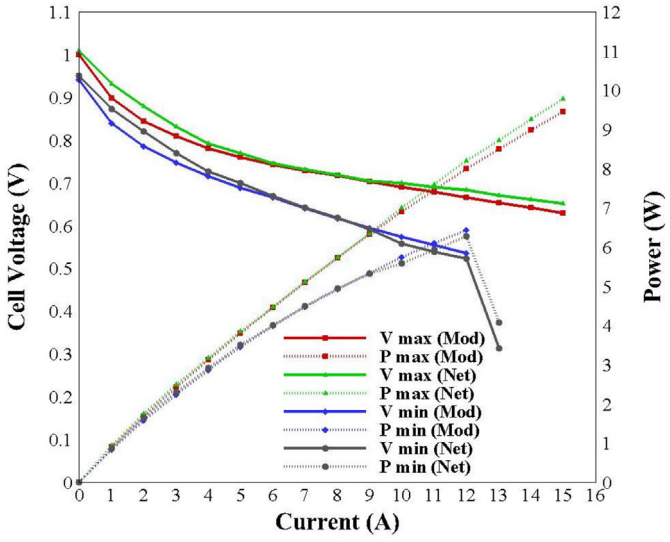

Fig. 7. Polarization power curves for maximum and minimum power.

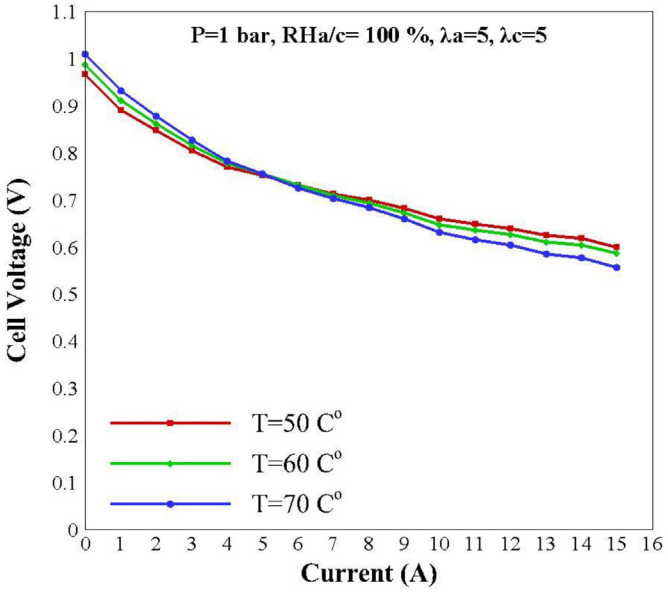

Fig. 8. Influence of operating temperature on the PEMFC performance.

PEMFC on the polarization curves at fixed operating conditions (P = 1 bar, $RH_{a/c}$ = 100%, $\lambda_a = 5$, $\lambda_c = 5$) for three temperatures (50 °C, 60 °C, and 70 °C). At low current densities, an increase in temperature improves the cell performance. Nevertheless, at high currents, an increased temperature gives the opposite result. This is so because as the temperature increases, the membrane ion conductivity is increased as well, which improves the diffusion of the hydrogen protons in the membrane. In addition, as the electrochemical reaction becomes faster, the water production in the cathode is increased which results in better hydration of the membrane. Accordingly, the membrane ionic resistance is reduced [46]. Then the performance of the cell is improved. At high current, an increased temperature imposes an increase in the water vapor partial pressure, which reduces the negative influence of flooding but it may also lead to membrane drying, which results in a decrease in ion conductivity. As a result, the performance of the cell decreases.

In Fig. 9, the influence of the relative humidity on the polarization curves of the PEMFC at a fixed operating condition (P = 1 bar, T = 70 °C, $\lambda_a = 5$, $\lambda_c = 5$) is depicted for three relative humidities (50%, 80% and 100%). By increasing the RH of the reactants, improvement of the performance is achieved. This is so as a change in the water mole fraction, due to the higher relative humidity of the inlet gases, increases the amount of water in the membrane. Then a reduction of the ionic resistance occurs and the proton movement is enhanced and accordingly the outlet current is increased at a certain voltage. As membrane drying is greater at higher temperatures, a higher inlet RH is contributing to the membrane hydration. For low currents, a change in the relative humidity does not affect the performance. In contrast, at high currents, a higher relative humidity improves the performance, as a considerable drop in the ohmic resistance occurs. These results agree with those presented in Ref. [47–49].

Fig. 10 provides the influence of the anode stoichiometry on the polarization curves of the PEMFC at fixed operating conditions (P = 1 bar, T = 70 °C, RH = 100%, $\lambda_c = 5$) for three anode stoichiometries (1.5, 3 and 5). It is observed that for all currents, increasing the anode stoichiometry improved cell performance, but the change is not so significant. Because this increase leads to increased hydrogen concentration, the electrochemical reaction rate is

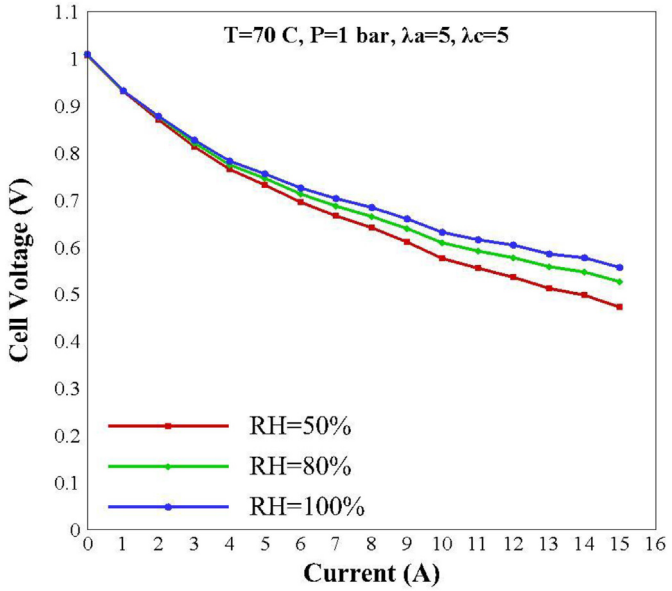

Fig. 9. Influence of relative humidity on the PEMFC performance.

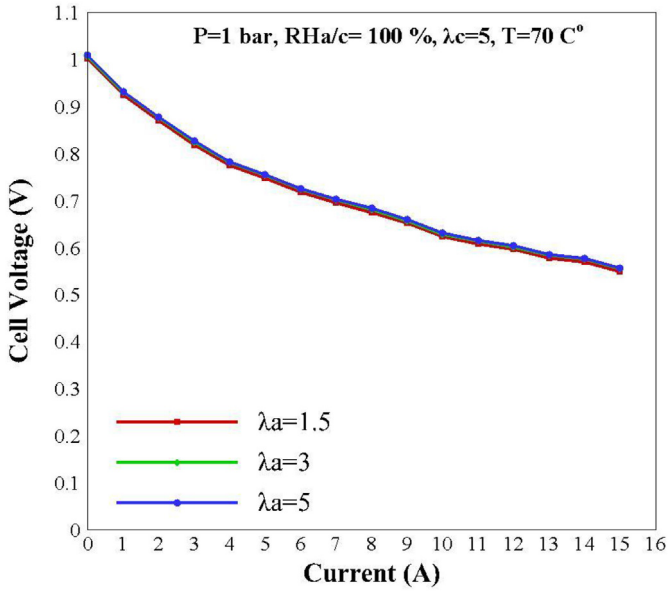

Fig. 10. Influence of anode stoichiometry on the PEMFC performance.

increased as well.

Fig. 11 provides the influence of cathode stoichiometry on the polarization curves of the PEMFC at fixed operating conditions (P = 1 bar, T = 70 °C, RH = 100%, λ_a = 5) for three cathode stoichiometries (2, 3 and 5). At low currents, a change in the cathode stoichiometry does not affect the cell performance. However, at high currents, a decrease of the cathode stoichiometry results in improvement of the cell performance. At low current, the cell is influenced significantly by the activation losses and it is found that cell performance is almost independent of the cathode stoichiometry. Limitations of the mass transport or concentration overpotentials appear when the reactants cannot be supplied sufficiently fast for the chemical reaction to take place. This may happen at high currents when a lot of liquid water is produced at the cathode [50], so for high currents, decreasing the cathode

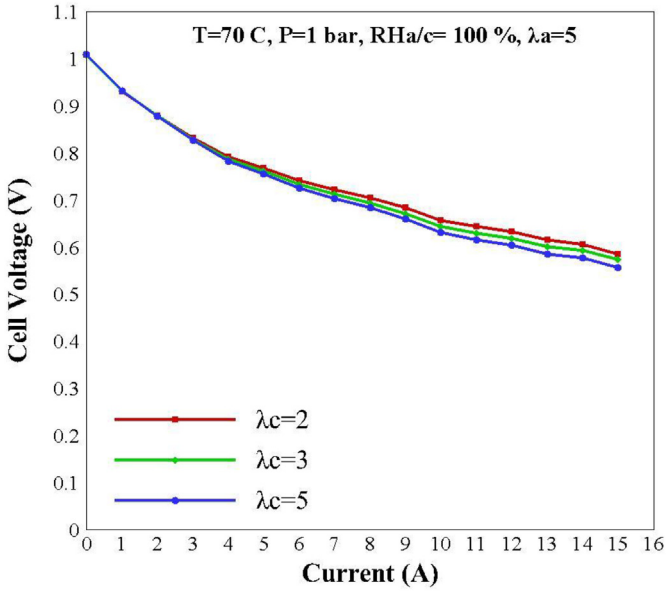

Fig. 11. Influence of cathode stoichiometry on the PEMFC performance.

stoichiometry improves the cell performance. In addition, in this situation, the concentration of water inside the duct increases faster and as a result, the membrane becomes humidified more quickly.

It must be noted that the conclusions of the proposed ANN model in this work may not be directly applicable in practice to any cell and operating conditions, as the properties and design of the cell components are obviously playing a fundamental influence on the operating conditions that lead to optimum performance. The analysis and discussions presented are corresponding to the range of operating conditions defined in Sections 6.2 and 6.3 together with the cell used (with components described in Salva et al. [27]). However, the methodology for the ANN model development presented in this work is applicable to any fuel cell and could be used to optimize the performance of the fuel cell being considered in each case.

7. Conclusions

An artificial neural network (ANN) approach was applied to maximize the output power of a PEMFC for various currents. Various operating conditions were considered, i.e., operating temperature, relative humidity, stoichiometry at cathode and anode sides at a constant pressure of 1 bar. For this particular case, the comparison between the operating condition of maximum performance with the operating condition of minimum performance at a reference current of 12 A, shows 23.6% (8.02 W versus 6.49 W) and 28.9% (8.16 W versus 6.33 W) increase of the power outputs by the model and the network, respectively.

As the network results presented a very good agreement with model results, as AARE was 1.95%, the network results were used to study the influence of the operating conditions on the PEMFC performance. The main conclusions are as follows:

1. For low currents, an increase of the temperature improved the performance of the cell, but for higher currents, the cell performance decreased as the partial pressure of water vapor was increased due to the increased temperature and membrane drying.

2. For low currents, the cell performance was relatively constant as the relative humidity was changed, but with increasing current, the cell performance was more perceptible to a change in relative humidity. Thus, as the relative humidity increases, due to the reduced charge transfer resistance, the cell performance was improved.
3. For all currents, increasing the anode stoichiometry improved the cell performance, but the change was not so significant. This improvement resulted in increased hydrogen concentration and then the electrochemical reaction rate was improved.
4. For low currents, a change of the cathode stoichiometry did not affect the cell performance. However, for high currents, the relative humidity was important. At high RH values, due to the mass transport limitations or concentration overpotentials, a decrease of the cathode stoichiometry improved cell performance. At low RH values, in general, it is better to increase the cathode stoichiometry as higher oxygen and water removal capability is achieved.

All the considered parameters in the model concerned the operating conditions of the PEM fuel cell, and therefore the power output was predicted only based on the optimum operating conditions. Optimization of the PEMFC performance based on design parameters will be in the scope of future investigations. The performance optimization is a key approach to achieve a cost reduction in PEMFCs, as more compact stacks can be achieved featuring a reduced number of cells for a given power output. The proposed ANN model revealed the maximum (or minimum) power output and the optimal operating conditions for any current, enabling the prediction of the optimal operation conditions for any current for achieving the maximum power output. The application of the ANN developed to the analysis of a PEMFC with MPL is also a novelty of this work.

CRediT authorship contribution statement

Fereshteh Salimi Nanadegani: Formal analysis, Investigation, Writing - original draft. **Ebrahim Nemati Lay:** Methodology, Supervision, Visualization, Writing - original draft. **Alfredo Iranzo:** Investigation, Methodology, Software, Validation, Writing - review & editing, Writing - original draft. **J. Antonio Salva:** Writing - original draft, Methodology, Software, Validation. **Bengt Sunden:** Formal analysis, Supervision, Writing - review & editing, Writing - original draft.

References

[1] K.Y. Chang, The optimal design for PEMFC modeling based on Taguchi method and genetic algorithm neural networks, Int. J. Hydrogen Energy 36 (21) (2011 Oct 1) 13683–13694.
[2] O.J. Murphy, A. Cisar, E. Clarke, Low-cost light weight high power density PEM fuel cell stack, Electrochim. Acta 43 (24) (1998 Aug 21) 3829–3840.
[3] K. Jayakumar, S. Pandiyan, N. Rajalakshmi, K.S. Dhathathreyan, Cost-benefit analysis of commercial bipolar plates for PEMFC's, J. Power Sources 161 (1) (2006 Oct 20) 454–459.
[4] X. Li, I. Sabir, Review of bipolar plates in PEM fuel cells: flow-field designs, Int. J. Hydrogen Energy 30 (4) (2005 Mar 1) 359–371.
[5] J.A. Salva, A. Iranzo, F. Rosa, E. Tapia, E. Lopez, F. Isorna, Optimization of a PEM fuel cell operating conditions: obtaining the maximum performance polarization curve, Int. J. Hydrogen Energy 41 (43) (2016 Nov 16) 19713–19723.
[6] M.M. Mench, Fuel Cell Engines, John Wiley & Sons, 2008 Mar 7.
[7] F. Barbir, PEM fuel cells, in: N. Sammes (Ed.), Fuel Cell Technology. Engineering Materials and Processes, Springer, London, 2006.
[8] S. Jemeı, D. Hissel, M.C. Péra, J.M. Kauffmann, On-board fuel cell power supply modeling on the basis of neural network methodology, J. Power Sources 124 (2) (2003 Nov 24) 479–486.
[9] S. JemeïJemei, D. Hissel, M.C. PÉraPera, J.M. Kauffmann, A new modeling approach of embedded fuel-cell power generators based on artificial neural network, IEEE Trans. Ind. Electron. 55 (1) (2008 Jan) 437–447.
[10] N.S. Sisworahardjo, T. Yalcinoz, M.Y. El-Sharkh, M.S. Alam, Neural network model of 100 W portable PEM fuel cell and experimental verification, Int. J. Hydrogen Energy 35 (17) (2010 Sep 1) 9104–9109.
[11] N.Y. Steiner, D. Hissel, P. Moçotéguy, D. Candusso, Diagnosis of polymer electrolyte fuel cells failure modes (flooding & drying out) by neural networks modeling, Int. J. Hydrogen Energy 36 (4) (2011 Feb 1) 3067–3075.
[12] C. Damour, M. Benne, J.J. Kadjo, S. Rosini, B. Grondin-Perez, Fast NMPC scheme of a 10 kW commercial PEMFC, Int. J. Hydrogen Energy 38 (18) (2013 Jun 18) 7407–7413.
[13] S. Curteanu, C.G. Piuleac, J.J. Linares, P. Cañizares, M.A. Rodrigo, J. Lobato, Neuro-evolutionary approach applied for optimizing the PEMFC performance, Int. J. Hydrogen Energy 39 (8) (2014 Mar 6) 4037–4043.
[14] I.S. Han, S.K. Park, C.B. Chung, Modeling and operation optimization of a proton exchange membrane fuel cell system for maximum efficiency, Energy Convers. Manag. 113 (2016 Apr 1) 52–65.
[15] L. Zhang, M. Pan, S. Quan, Model predictive control of water management in PEMFC, J. Power Sources 180 (1) (2008 May 15) 322–329.
[16] C. Lebreton, M. Benne, C. Damour, N. Yousfi-Steiner, B. Grondin-Perez, D. Hissel, J.P. Chabriat, Fault tolerant control Strategy applied to PEMFC water management, Int. J. Hydrogen Energy 40 (33) (2015 Sep 7) 10636–10646.
[17] Y.P. Chang, Optimal design of operation parameters on performance of PEMFC, J. Mar. Sci. Technol. 24 (4) (2016 Aug 1) 702–710.
[18] A. Mawardi, F. Yang, R. Pitchumani, Optimization of the operating parameters of a proton exchange membrane fuel cell for maximum power density, J. Fuel Cell Sci. Technol. 2 (2) (2005 May 1) 121–135.
[19] S. Kaytakoğlu, L. Akyalçın, Optimization of parametric performance of a PEMFC, Int. J. Hydrogen Energy 32 (17) (2007) 4418–4423. F Dec 1.
[20] A. Askarzadeh, A. Rezazadeh, Optimization of PEMFC model parameters with a modified particle swarm optimization, Int. J. Energy Res. 35 (14) (2011 Nov) 1258–1265.
[21] V. Meidanshahi, G. Karimi, Dynamic modeling, optimization and control of power density in a PEM fuel cell, Appl. Energy 93 (2012 May 1) 98–105.
[22] C. Zhang, W. Zhou, M.M. Ehteshami, Y. Wang, S.H. Chan, Determination of the optimal operating temperature range for high temperature PEM fuel cell considering its performance, CO tolerance and degradation, Energy Convers. Manag. 105 (2015 Nov 15) 433–441.
[23] H. Kanani, M. Shams, M. Hasheminasab, A. Bozorgnezhad, Model development and optimization of operating conditions to maximize PEMFC performance by response surface methodology, Energy Convers. Manag. 93 (2015 Mar 15) 9–22.
[24] Z.J. Mo, X.J. Zhu, L.Y. Wei, G.Y. Cao, Parameter optimization for a PEMFC model with a hybrid genetic algorithm, Int. J. Energy Res. 30 (8) (2006 Jun 25) 585–597.
[25] D. Liu, S. Xia, H. Tang, D. Zhong, B. Wang, X. Cai, R. Lin, Parameter optimization of PEMFC stack under steady working condition using orthogonal experimental design, Int. J. Energy Res. (2018 Jul 17) 1–12, special issue.
[26] R. Petrone, Z. Zheng, D. Hissel, M.C. Péra, C. Pianese, M. Sorrentino, M. Becherif, N. Yousfi-Steiner, A review on model-based diagnosis methodologies for PEMFCs, Int. J. Hydrogen Energy 38 (17) (2013 Jun 10) 7077–7091.
[27] J.A. Salva, A. Iranzo, F. Rosa, E. Tapia, Validation of cell voltage and water content in a PEM (polymer electrolyte membrane) fuel cell model using neutron imaging for different operating conditions, Energy 101 (2016 Apr 15) 100–112.
[28] NeuroSolutions. http://www.neurosolutions.com/.
[29] W.R. Daud, E.H. Majlan, M.I. Rosli, Water balance for the design of a PEM fuel cell system, Int. J. Hydrogen Energy 38 (22) (2013 Jul 26) 9409–9420.
[30] A. Iranzo, P. Boillat, P. Oberholzer, J. Guerra, A novel approach coupling neutron imaging and numerical modelling for the analysis of the impact of water on fuel cell performance, Energy 68 (2014 Apr 15) 971–981.
[31] M.H. Akbari, B. Rismanchi, Numerical investigation of flow field configuration and contact resistance for PEM fuel cell performance, Renew. Energy 33 (8) (2008 Aug 1) 1775–1783.
[32] C. Ziogou, S. Voutetakis, S. Papadopoulou, M.C. Georgiadis, Modeling, simulation and experimental validation of a PEM fuel cell system, Comput. Chem. Eng. 35 (9) (2011 Sep 14) 1886–1900.
[33] ElectroChem. Inc. http://fuelcell.com/techsheets/Brochure%20FC05&25.pdf.
[34] SGL Group. http://www.sglgroup.com/cms/international/products/productgroups/su/fuel-cell-components/.
[35] QuinTech Fuel Cell Technology. http://www.quintech.de/englisch/pdf/catalog/fuel-cells-components-applications.pdf.
[36] T.E. Springer, T.A. Zawodzinski, S. Gottesfeld, Polymer electrolyte fuel cell model, J. Electrochem. Soc. 138 (8) (1991 Aug 1) 2334–2342.
[37] H.A. Gasteiger, S.G. Yan, Dependence of PEM fuel cell performance on catalyst loading, J. Power Sources 127 (1–2) (2004 Mar 10) 162–171.
[38] S.O. Ogaji, R. Singh, P. Pilidis, M. Diacakis, Modelling fuel cell performance using artificial intelligence, J. Power Sources 154 (1) (2006 Mar 9) 192–197.
[39] S. Haykin, Neural Neural Network and its Application in IR, a Comprehensive Foundation, vol. 13, New Jersey: Prentice Hall, Upper Saddle Rever, 1999, pp. 775–781, 842p.
[40] M. Ohenoja, K. Leiviskä, Validation of genetic algorithm results in a fuel cell model, Int. J. Hydrogen Energy 35 (22) (2010 Nov 1) 12618–12625.
[41] A. Majdi, M. Beiki, Evolving neural network using a genetic algorithm for predicting the deformation modulus of rock masses, Int. J. Rock Mech. Min. Sci. 47 (2) (2010 Feb 1) 246–253.
[42] A. Mohebbi, M. Taheri, A. Soltani, A neural network for predicting saturated

liquid density using genetic algorithm for pure and mixed refrigerants, Int. J. Refrig. 31 (8) (2008 Dec 1) 1317–1327.
[43] J.J. Baschuk, X. Li, Modelling of polymer electrolyte membrane fuel cells with variable degrees of water flooding, J. Power Sources 86 (1–2) (2000 Mar 1) 181–196.
[44] S. Um, C.Y. Wang, K.S. Chen, Computational fluid dynamics modeling of proton exchange membrane fuel cells, J. Electrochem. Soc. 147 (12) (2000 Dec 1) 4485–4493.
[45] L. Wang, A. Husar, T. Zhou, H. Liu, A parametric study of PEM fuel cell performances. ASME 2002 International Mechanical Engineering Congress and Exposition, American Society of Mechanical Engineers, 2002 Jan 1, pp. 139–145.
[46] Z. Belkhiri, M. Zeroual, H.B. Moussa, B. Zitouni, Effect of temperature and water content on the performance of PEM fuel cell, Revue des Energies Renouvelables 14 (1) (2011) 121–130.
[47] J. Zhang, Y. Tang, C. Song, Z. Xia, H. Li, H. Wang, J. Zhang, PEM fuel cell relative humidity (RH) and its effect on performance at high temperatures, Electrochim. Acta 53 (16) (2008 Jun 30) 5315–5321.
[48] H. Sabadbafan, Effect of humidity content and direction of the flow of reactant gases on water management in the 4-serpentine and 1-serpentine flow channel in a PEM (proton exchange membrane) fuel cell, Energy 101 (2016 Apr 15) 252–265.
[49] F. Salimi Nanadegani, E. Nemati Lay, B. Sunden, Effects of an MPL on water and thermal management in a PEMFC, Int. J. Energy Res. 43 (2018) 274–296.
[50] D. Cheddie, N. Munroe, Review and comparison of approaches to proton exchange membrane fuel cell modeling, J. Power Sources 147 (1–2) (2005 Sep 9) 72–84.

Nomenclature

Abbreviations

ANN: artificial neural network
BP: Bipolar Plate
CL: Catalyst Layer
DE: Differential evolution
EES: Engineering Equation Solver
FTCS: Fault Tolerant Control Strategy
GDL: Gas Diffusion Layer
HGA: Hybrid Genetic Algorithm
MLP: Multi-layer feed-forward networks
MPL: Micro Porous Layer
MPSO: Modified Particle Swarm Optimization
PEM: Polymer Electrolyte Membrane
PEMFC: Polymer Electrolyte Membrane Fuel Cell
RNN: Recurrent Neural Network
SNAOA: Sequential Neural-network Approximation and Orthogonal Arrays

Symbols

a: water activity
$C^{mem}_{H_2O,i}$: water concentration in the membrane in anode and cathode (mol/m^3)
$C_{i,GDL-CL}$: hydrogen or oxygen concentration at the GDL-CL interface of the anode or cathode (mol/m^3)
C_{ref}: reference concentration (mol/m^3)
$E_{a,i}$: activation energy in anode and cathode (J/mol)
$E^0(T,P)$: theoretical equilibrium open-circuit potential of the cell (V)
F: Faraday constant (96,487 C/mol)
i: current density (A/m^2)
$i_{lim,i}$: limiting current density in anode or cathode (A/m^2)
$i_{0,i}$: exchange current density in anode and cathode (A/m^2)
$i_{ref,i}$: reference exchange current density in anode and cathode (A/m^2)
G: Gibbs free energy (J)
n_i: equivalent electrons per mole of reactant (2 for anode side and 4 for cathode side)
P^0: reference pressure (Pa)
P_{sat}: saturation pressure (Pa)
$P_{anode/cathode}$: operating pressure in anode and cathode (Pa)
R: constant of the ideal gases (8.314 J/mol K)
$R_{contact}$: contact resistance between the GDL and the BP (Ωm^2)
RH: Relative humidity
T: operating temperature (T)
t_i: Thickness (m)
V_{cell}: output voltage (V)
y_i: mole fraction of hydrogen, water and oxygen in anode and cathode

Greek letters

α_i: charge transfer coefficient in anode and cathode
γ_i: reaction order for the elementary charge transfer step
$\eta_{a,i}$: activation overpotentials in anode and cathode (V)
$\eta_{m,i}$: concentration overpotentials in anode and cathode (V)
η_r: ohmic overpotential (V)
λ: water content inside the membrane
σ_i: electrical conductivity (1/ Ωm)